Effect of Electrode Diameter and Current on Dissimilar Metal Welding (Stainless Steel - Galvanized Steel) in Bus Body Construction: Microstructure and Properties Evaluation

Suntari[1], **Helmy Purwanto**[1] ✉, **Sri Mulyo Bondan Respati**[1], **Sugiarto**[2], **Zainal Abidin**[3]

[1]Department of Mechanical Engineering, Faculty of Engineering, Universitas Wahid Hasyim, 50236, Indonesia
[2]Department of Mechanical Engineering, Faculty of Engineering, Brawijaya University, 65145, Indonesia
[3]Southwest Research Institute, San Antonio, Texas 78238, United States

✉ helmypurwanto@unwahas.ac.id

Abstract

This study evaluates the macrostructure, microstructure, hardness, and tensile strength in dissimilar metal welding applied to bus body construction. The process involved joining hollow stainless steel and galvanized steel at the dimensions of 80 x 40 x 3.2 mm through Gas Metal Arc Welding (GMAW). The current was varied at 90, 100, and 110 A while ER70S-6 electrodes with diameters of 0.8 and 1.0 mm were used. The results showed that electrode diameter and welding current affect the capping area, penetration depth, and hardness. Moreover, the formation of the widmasatten ferrite phase was increased and the coarse grain boundaries in the weld zone were detected. It was also observed that an increase in the diameter of the electrode and the welding current which indicates an increment in the heat reduced the rate of solidification and cooling. The average tensile strength for all the samples investigated was found to be lower than the value for the base metal. Therefore, further research is recommended to improve the tensile strength.

Keywords: Dissimilar welding, Material properties, Body bus construction

1. Introduction

There is a need to ensure adequate land transportation through the procurement of vehicles produced with robust and high quality in order to achieve safety and comfort. This means the car or bus body building industry which specializes in the manufacturing of public passenger vehicle bodies needs greater attention. This is mostly related to the assurance of quality in the design and construction processes in order to guarantee the safety of passengers and also provide light weight [1], [2]. It is, however, important to note that the different kinds of materials usually applied to ensure safety and lightweight normally present challenges in the process of joining and welding [3]. The most common is the welding of joints between stainless steel and galvanized steel as observed in the inner frame of the cross member supporting the bus body. This is better known as the dissimilar material weld joint.

The demand for dissimilar material welding in constructions, especially during the manufacture of vehicle bodies, is increasing due to its lower cost. Alloy steels such as stainless steel are relatively expensive and are usually required to be welded on the other side with carbon steel which is relatively less costly [4], [5]. Meanwhile, stainless steel is needed in parts associated with high corrosion rates but the joining of dissimilar materials poses challenges in achieving a quality connection [6]–[10]. This is mostly because there is a need for the two metals to be welded to be soluble with each other while the filler metal also needs to be easily soluble with the base metal in order to obtain the desired strength [9], [11].

It was reported that the mechanical strength obtained from welding dissimilar materials such as twinning-induced plasticity (TWIP) steel, austenitic stainless steel (ASS) AISI 304 L, and duplex stainless steel (DSS) 2205 decreased due to the planar solidification growth detected in the fusion zone and heat affected zone interface [12]. In addition to mechanical problems, several other metallurgical problems were also found such as the formation of destructive secondary phases, carbon diffusion-related problems, δ-ferrite phase present in the fusion zone, and residual stresses [13], [14]. Furthermore, solidification cracks, hydrogen cracks, and the formation of brittle phases have the ability to cause component failure before the expected service life [15].

The dissimilar welding conducted using laser oscillation welding was, however, reported to have the ability to produce welds with tensile strength and high precision [16], [17]. The addition of an interlayer Ni on the laser welding of cupper-stainless steel was observed to have prevented the formation of welding defects and spherical particles and also improved the mechanical properties of the joint [17]. Meanwhile, this method requires high costs and energy and this means it is not suitable for medium-sized manufacturing industries. This is the reason Shield Metal Arc Welding (SMAW) and Gas Metal Arc Welding (GMAW) are more widely used in the automotive or bus body building industry.

GMAW is a type of welding that is familiar in the construction field, especially in the automotive industry. It is suitable for welding similar materials but usually encounters certain obstacles with dissimilar materials. The quality of its results is normally determined by the welding current settings and the use of the right electrode. For example, Anuradha et al. [6] reported that the use of Inconel-based electrodes produced better joint tensile strength compared to stainless steel-based electrodes. This is due to the fact that different types of electrodes affect the composition in the connection zone [18] and subsequently the microstructure and properties.

Welding current, voltage, speed settings, type of electrode, electrode angle, bevel angle, and root gap in the GMAW process can be used to obtain optimal welding strength and determine metal deposition rate [19]. The welding current is the main parameter to suppress the impact force of the weld joint followed by the welding voltage [20]. This was confirmed by Arora et al. [19] that heat input changes the microstructure of the base material into HAZ and weld pool. This parameter setting also minimizes the possibility of service failure of welded joints in dissimilar materials [21].

The technology to improve the mechanical performance of joining multi-materials in the automotive industry is limited and this means there is a need to develop the appropriate ones to meet these needs [22]. It was discovered from literature studies that joints of dissimilar materials have been widely welded using GMAW. However, the effect of the types of filler wire diameter or welding electrode used on the weld results has not been widely reviewed. It is important to note that galvanized steel is steel coated with zinc because it has a much lower melting point. Therefore, the zinc element is likely to be an impurity and its effect on the welding results needs to be studied. Moreover, the filler wire diameter influences the current resistance and this further affects the heat input to the metal. The purpose of this study was to determine and analyze the microstructure and mechanical properties of dissimilar material connections using GMAW welding at different variations of filler wire diameter and welding current. This is important because there are different forms of welding applications in the automotive industry, including the bus body construction sector, and the filler wire diameter selected has the ability to influence the production costs in terms of the material and time.

2. Materials and Method

The dissimilar materials used in this study were hollow square stainless steel 304 and galvanized steel STKM 13B on the inner frame of the bus cross member supporting the bus body. Their dimension is 80.0 x 40.0 mm with a thickness of 3.20 mm and their composition is presented in **Table 1** while their mechanical properties are listed in **Table 2**.

The materials were prepared for the welding according to ISO 5817 [23] as shown in **Figure 1**. The process was conducted using the GMAW (Focus® MAG 353 S) with Direct Current Electrode Positive (DCEP) polarity through the application

of ER70S-6 filler electrode at 0.8 and 1.0 mm diameters and with the chemical composition indicated in **Table 1**. Moreover, the welding machine was set up at different welding currents of 90, 100, and 110 A with each repeated and tested 3 times using the sample codes presented in **Table 3**.

The welding bevel was shaped into V-groove at an angle of 30°, root face of 1 mm, and root gap of 1 mm. The voltage used was 20 volts with a welding speed of 3.5 mm/s, 1-G welding position, and two welding steps. Moreover, the shield gas was set at a composition of 80% Ar and 20% CO_2 with a flow volume of 15 liters/min [23].

Table 1. Chemical composition of materials and electrode filler

Material	Chemical Composition (% wt.)										
	C	Si	Mn	P	S	Cr	Ni	Mo	Cu	V	Fe
Stainless steel 304	0.042	0.42	1.190	0.021	0.001	16.80	8.400	-	-	-	Bal.
Galvanized STKM 13B	0.188	0.164	0.393	0.041	0.014	0.073	0.022	0.002	0.002	-	Bal.
Electrode ER70S-6 [24]	0.150	1.032	1.831	0.018	0.031	0.011	0.013	0.010	0.432	0.007	Bal.

Table 2. Mechanical properties of the material [25]

Material	Tensile strength (MPa)	Melting Point (°C)	Density (gr/cm3)	Poisson's Ratio	Modulus of Elasticity (GPa)	Coefficient of Thermal Expansion 10-6 (°C)-1	Thermal Conductivity (W/m · K)	Specific Heat (J/kg·K)	Electrical Resistivity (Ω· m)
Stainless steel 304	507.620	1450	8	0.3	193	17.2	16.2	500	7.2×10^{-7}
Galvanized STKM 13B	505.884	1425	7.85	0.3	207	11.7	51.9	486	1.60×10^{-7}

Table 3. Research variables and specimen codes

| No	Variable	Heat Input (J/mm) [26]	Code
1	Stainless steel base metal	-	SS
2	Galvanized base metal	-	GS
3	Filler wire diameter (electrode) 0.8 mm with a current of 90A	437.143	W1
4	Filler wire diameter (electrode) 0.8 mm with a current of 100A	485.714	W2
5	Filler wire diameter (electrode) 0.8 mm with a current of 110A	534.285	W3
6	Filler wire diameter (electrode) 1.0 mm with a current of 90A	437.143	W4
7	Filler wire diameter (electrode) 1.0 mm with a current of 100A	485.714	W5
8	Filler wire diameter (electrode) 1.0 mm with a current of 110A	534.285	W6
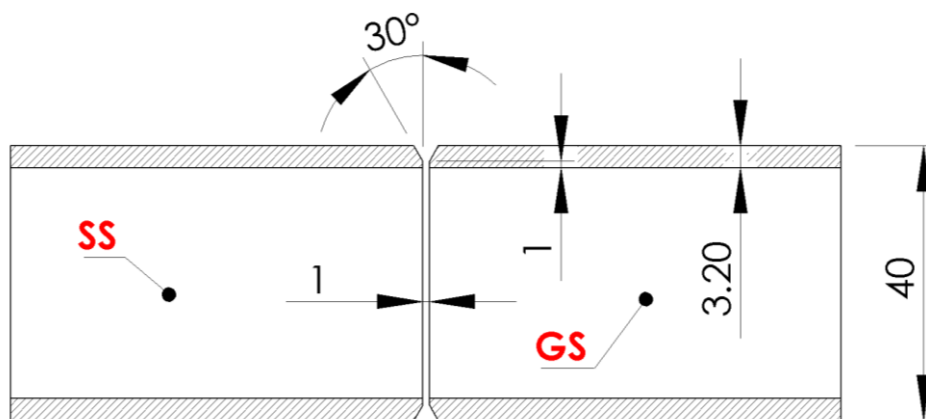
Figure 1. Preparation of materials to be welded according

The welding results were physically observed using a macro (Digital Opticon Digeye®), metallurgical microscope (Krisbow® SKU KW0600592), and Scanning Electron Microscope-Energy Dispersion Spectroscopy (SEM-EDS) Phenom ProX® Thermo Scientific Gen-6. Meanwhile, the micro-grain analysis was conducted using the ImageJ application software and the grain size number was calculated according to ASTM E112 [27]. The hardness was tested using the Rockwell B-scale (Krisbow® KW0600121) with an indentation load of 90 N while the tensile strength was determined through a universal testing machine Gotech® GT-701-LC10 with a maximum capacity of 10 tons and a tensile speed of 15 mm/s. The tensile test specimen was made according to ASTM E8 [28] as shown in **Figure 2** and each test on each variable or zone was repeated 3 times.

3. Results and Discussion

3.1. Macrostructure

The metallography of the welding results obtained from using the GMAW method on each research variable is presented in **Figure 3** with the observation area divided into three zones which include the base metal (BM), heat affected zone (HAZ), and weld metal (WM). The BM is the area not affected by the welding process and this means its properties remain the same before and after the joining. The HAZ is the base metal whose properties change due to the influence of welding heat but the metal in this zone did not melt. Meanwhile, the WM is the result obtained from solidifying an alloy of base metal and filler metal. Therefore, its properties are very different from BM and HAZ.
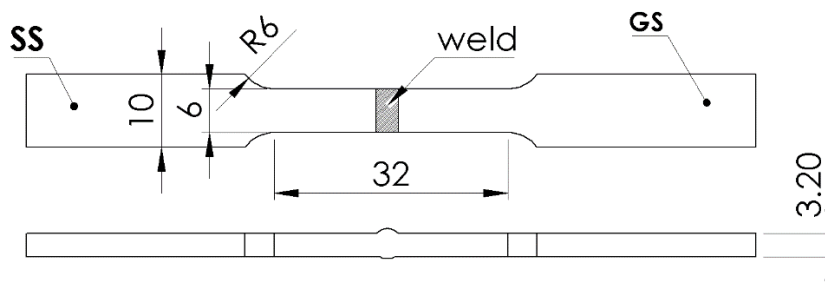

Figure 2. Dimensions of the tensile test specimen according to ASTM E8 [28]
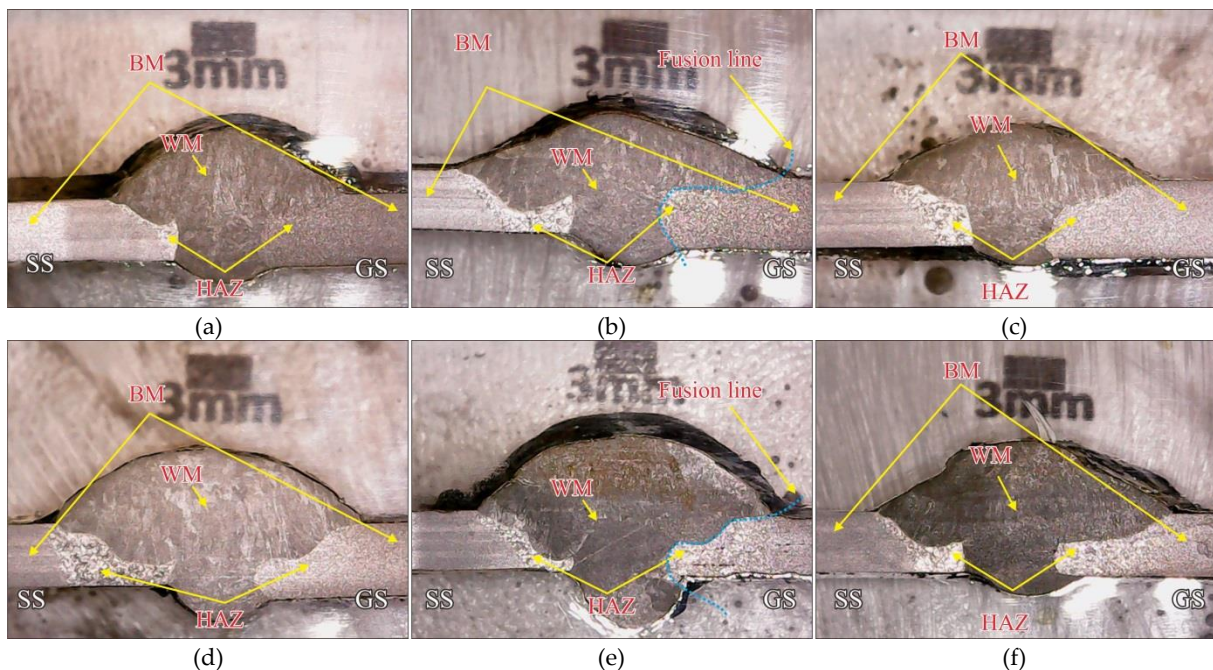

Figure 3. Welding metallography (a) Specimen code W1, (b) Specimen code W2, (c) Specimen code W3, (d) Specimen code W4, (e) Specimen code W5, and (f) Specimen code W6

The shape, capping width, and weld penetration in **Figure 3** show that larger electrode diameter and current produced wider capping and weld penetration. This is due to higher heat input received by the sample from these parameters which further led to greater melting of base metal and filler. The high heat input also caused large distortion, especially on thin plates, due to the difference between the heat and an uneven distribution of thermal stresses in the metals being welded. This is in line with the report of Demarque et al. [29] that heat input usually affects physical and mechanical characters and is required to be optimal in order to prevent lack of fusion defects such as incomplete melting caused by low heat and a larger weld pool by excessively high heat [30]. W1, which is the specimen with 0.8 mm diameter and 90 A current in **Figure 3a**, shows that the penetration of the HAZ and the root is rather shallow while the width of the capping is smaller than that of the W2 with 100 A current and 0.8 mm electrode diameter in **Figure 3b**.

3.2. Microstructure

The microstructure of stainless-steel base metal and galvanized steel is presented in **Figure 4**. The stainless-steel structure consists of ferrite and austenite structures while the galvanized steel has ferrite and perlite structures.

The microstructure of stainless steel presented in **Figure 4a** showed that the visible austenite structure (dark) was formed due to the presence of Cr, Ni, and Mn content presented in **Table 1**. It is also an austenitic stainless steel 304 [31], [32]. Meanwhile, the ferrite (α-Fe) (bright) structure was formed because the main composition is Fe. It

was also observed that the galvanized steel microstructure looks like ferrite and perlite structures as indicated in **Figure 4b**. The perlite aspect was due to the existence of lamination between cementite and ferrite or the eutectoid alloy of ferrite and cementite [25] which is caused by the fact that the galvanized base metal is low-carbon steel.

The microstructure of the Heat Affected Zone (HAZ) at the stainless-steel side of each variable is presented in **Figure 5**. It was observed to be obtained in the area close to the fusion line and this makes the grain to look coarser which is also known as the coarse grain zone. In this zone, the phase changed to the austenite as indicated in **Figure 3** because the temperature received during welding reached 1100-1200°C [33].

The HAZ is the zone near the weld metal but which did not melt and the part on the stainless-steel showed acicular ferrite (AF), Widmanstatten ferrite (WF), and grain boundary ferrite (GBF) structures for all the variations. The acicular ferrite is a structure formed intra-granularly at a small size in random directions due to the influence of a fairly low temperature from the welding process. The widmanstatten ferrite was formed along the ferrite grain boundary with a flake-like shape and tends to be parallel to the ferrite grain boundary [26]. It is important to note that greater current led to higher heat input and this subsequently caused the formation of more WF because its patterns are usually formed at a fairly high temperature compared to acicular ferrite. **Figure 5c** shows more widmanstatten patterns at 110A current compared to **Figure 5a**

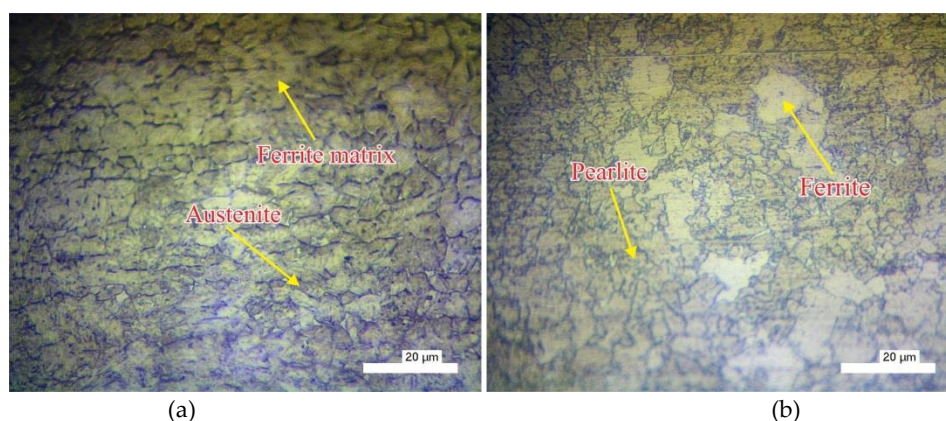|	
(a)	(b)

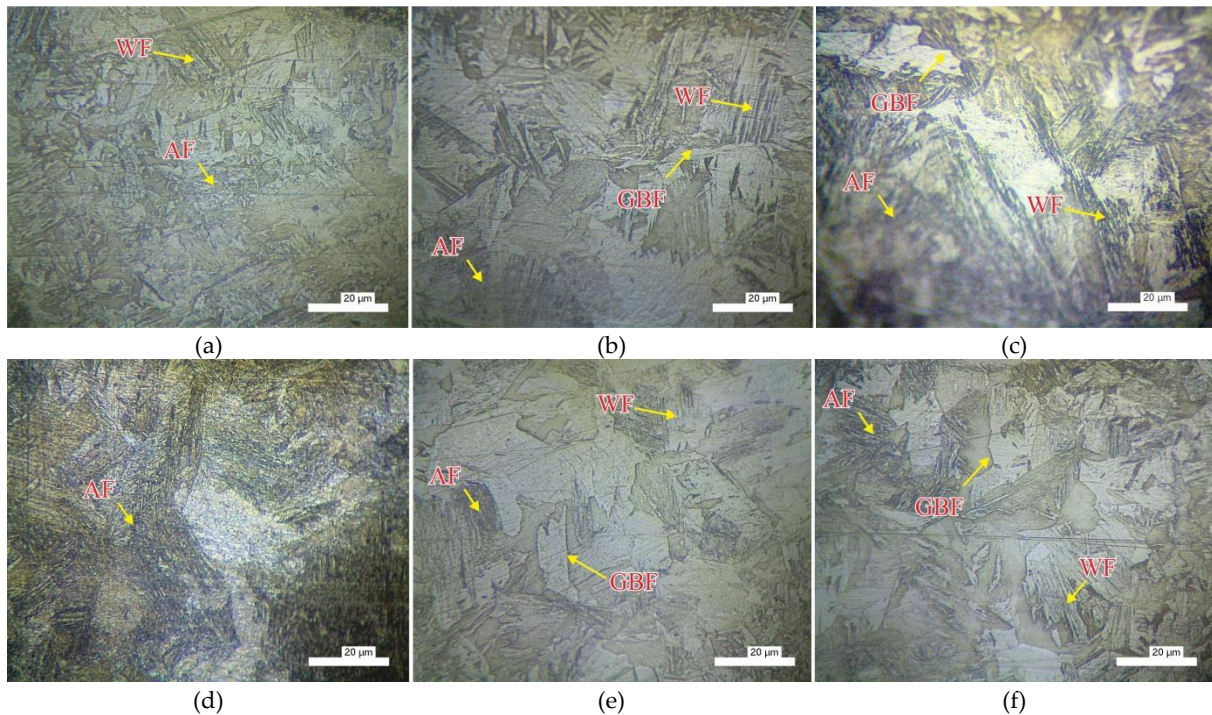**Figure 4.** Microstructure (a). Stainless steel and (b). galvanized steel

Figure 5. The microstructure of the HAZ of stainless-steel (a) Specimen code W1, (b) Specimen code, (c) Specimen code W3, (d) Specimen code W4, (e) Specimen code W5, and (f) Specimen code W6

with 90 A current. It was similarly reported by Hamd et al. [34] that an increase in the weld heat input increased the width of weld metal and heat-affected zone, and this led to a reduction in the impact energy. Moreover, grain coarsening was experienced in the bainite-martensite proportion due to the increase in heat input [35].

The microstructure of the HAZ on the galvanized steel side is presented in **Figure 6** and WM in **Figure 7**. It was discovered in the HAZ of the galvanized steel for the filler wire with 0.8 mm diameter and 90, 100, and 110A currents that ferrite (F) and pearlite (P) structures are visible as indicated in **Figure 6a**, **Figure 6b,** and **Figure 6c** while widmanstatten ferrite structures were only observed with 0.8 mm and 110A treatment as presented in **Figure 6c**. Moreover, acicular ferrite was reported with the usage of 1.0 mm diameter and 90A current in **Figure 6d** while widmanstatten ferrite was observed more and more with 1.0 mm diameter with 100 and 110 A current in **Figure 6e** and **Figure 6f**. It is important to note that the HAZ structures of galvanized and stainless steel are similar due to the greater heat input produced through the increase in the welding current and filler wire diameter.

It was discovered that the martensite-bainite structure is dominantly visible in the weld metal.

It is different from the HAZ structure and base metal due to the addition of filler metal. The temperature used during the welding was able to melt the base metal and filler, and the grain was getting coarser due to the use of bigger filler wire diameters at increased current as shown in **Figure 7a** and **Figure 7f**). This is because a higher current and wider diameter produced greater heat input on the metal to reduce the solidification and cooling processes of the weld metal.

The Scanning Electron Microscope-Energy and Dispersion Spectroscopy (SEM-EDS) results of the BM, HAZ, and WM regions are presented in **Figure 8**. It was discovered that the stainless-steel BM has porosity, impurities, and a $Cr - Mn$ matrix as indicated in **Figure 8a**. Moreover, the EDS test detected 13,700% Cr, 1,400% Mn (%wt.), and Fe balance in the austenite section (dark). The stainless steel HAZ also shows acicular ferrite (AF), widmanstatten ferrite (WF), and grain boundary ferrite (GBF) structures as presented in **Figure 8b**. The FGB was formed along the grain and is lighter in color. Furthermore, the EDS test also showed an alloy composition of 13.786% Cr, 1,598 Mn (%wt.), and Fe balance. It was discovered that there was a change in the structure between the parent metal and HAZ but the elemental content was relatively the same.
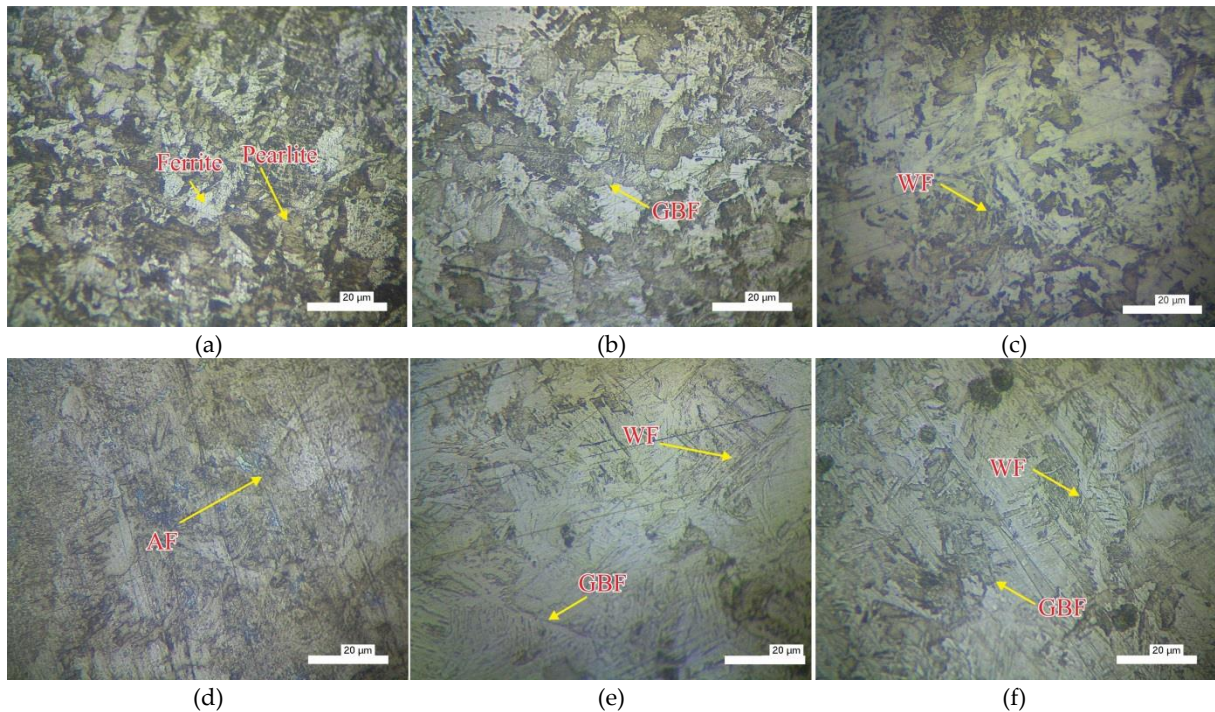
Figure 6. The microstructure of the HAZ of galvanized steel (a) Specimen code W1, (b) Specimen code, (c) Specimen code W3, (d) Specimen code W4, (e) Specimen code W5, and (f) Specimen code W6
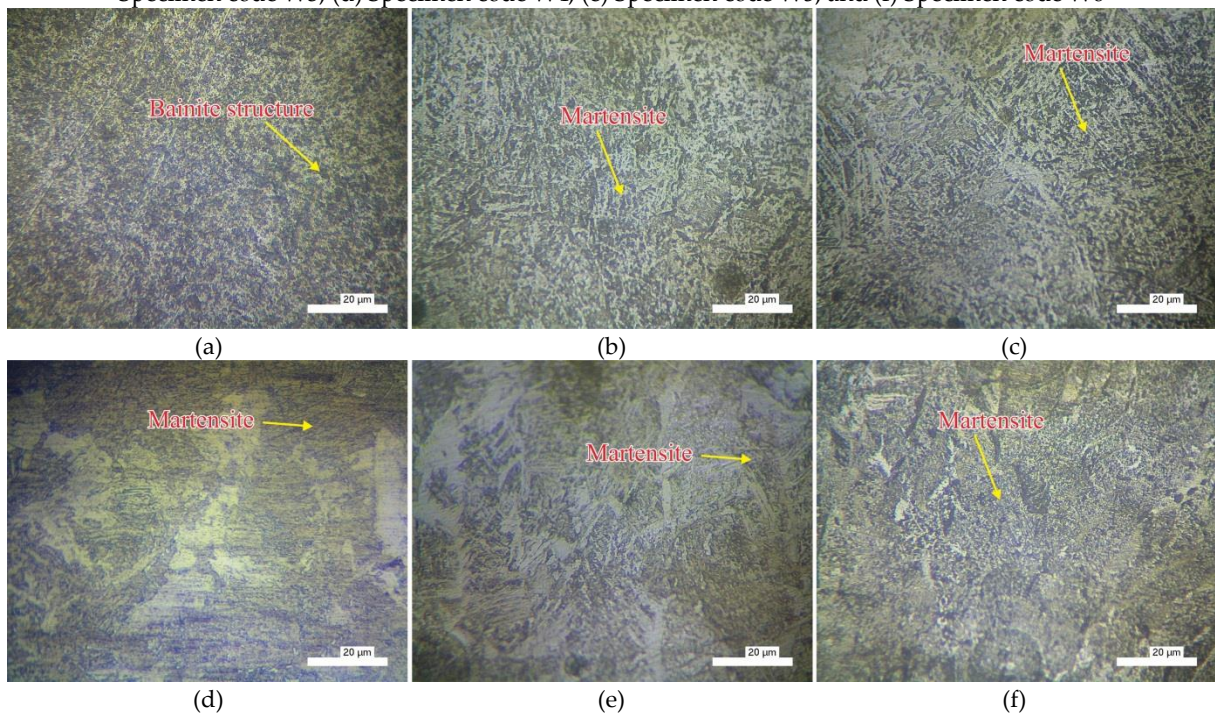

Figure 7. The microstructure of the weld metal (a) Specimen code W1, (b) Specimen code, (c) Specimen code W3, (d) Specimen code W4, (e) Specimen code W5, and (f) Specimen code W6

This proves that there is no addition of HAZ elements from outside. The structural changes were associated with the welding heat that reached the austenite temperature and sustained by the influence of the cooling rate which led to recrystallization.

The microstructure of the weld metal presented in **Figure 8c** is observed to be different because it is formed through the solidification of the molten parent metal and filler. The EDS test results also showed the existence of 1.602% C, 0.501% Si, 1.802% Cr, 3.203% O (%wt.), and Fe
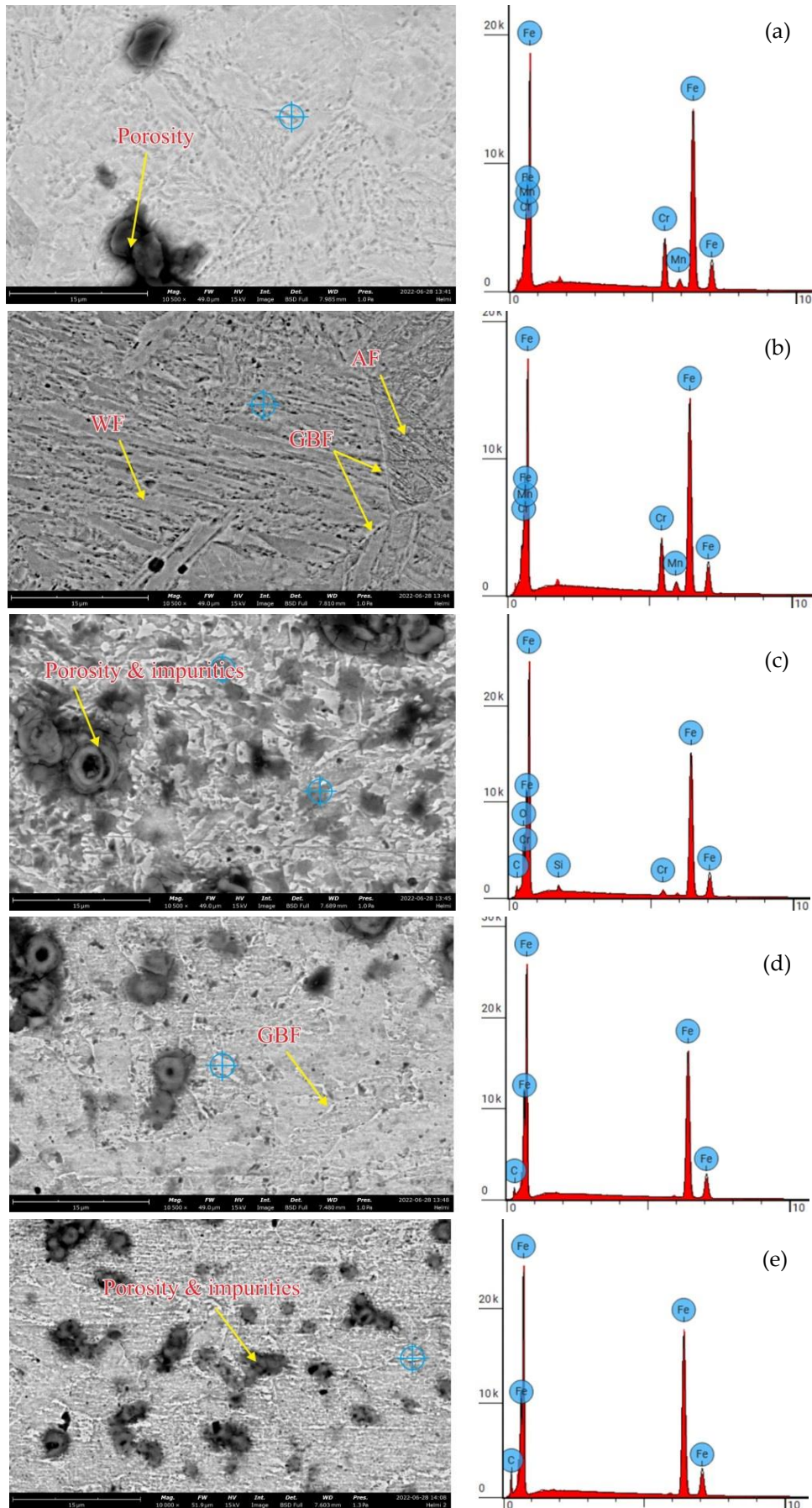
Figure 8. SEM and EDS on (a) base metal stainless steel, (b) HAZ stainless steel, (c) weld metal, (d) HAZ galvanize steel, and (e) base metal galvanize steel

balance. The weld metal was indicated by the Si content in the filler wire as presented in **Table 2**. Meanwhile, the HAZ on the galvanized steel as well as porosity was observed to be visible in GBF as shown in **Figure 8d**. The elemental content of the galvanized steel HAZ was found to include 2.705% C (% wt.) and Fe. Similarly, the galvanized steel BM has 3.410 % C (% wt.) and Fe. The findings also showed porosity and impurity in each zone, especially the weld metal. The porosity was associated with the trapped air when the molten metal solidified.

The average grain size was presented in **Figure 4**, **Figure 5**, and **Figure 6** while the grain size numbers on the BM and HAZ are presented in **Figure 9**. Meanwhile, the WM was difficult to measure because the grain boundaries were blocked by the martensite-bainite structure in the form of lath and needles.
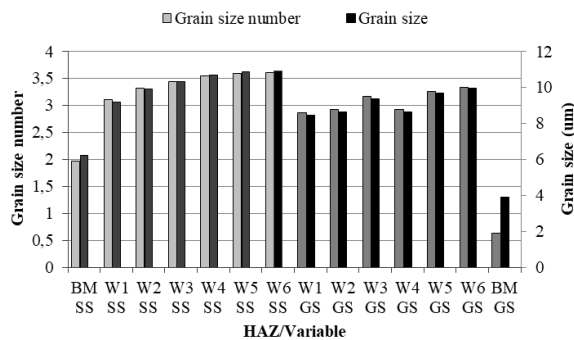

Figure 9. Grain size number and average grain size of base metal and HAZ

The grain size number of stainless steel was observed to be relatively larger than galvanized steel. This was indicated by the 1.97 or average of 6.21 μm and 0.64 or average of 3.91 μm for their BM respectively. It was also discovered that both grain shapes on the base metal were relatively oval because the material was produced by rollers. Meanwhile, the smallest grain size number in the stainless steel HAZ was found in the W1 sample at 3.10 or an average of 9.20 μm and looked coarser up to 3.60 or an average of 10.92 μm in the W6 sample. A similar trend was observed for the galvanized steel HAZ with the W1 sample having 2.86 or an average of 8.44 μm and the value was increasing up to the W6 sample with 3.34 or an average of 9.98 μm. This means the average grain size for HAZ in stainless steel was larger than galvanized steel in each sample. This change was associated with the recrystallization process caused by the influence of the welding heat that

reached the austenite temperature. This means higher heat input received by the metal reduced the cooling rate and subsequently made the grain size coarser or larger.

3.3. Hardness

The hardness of the samples was tested using the Rockwell scale B method and the results are presented in **Figure 10**.
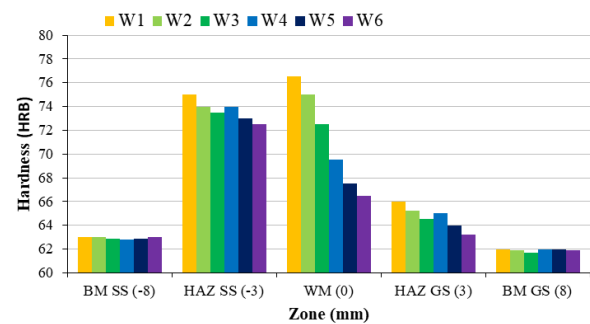

Figure 10. Average hardness values for base metal (BM) SS and Galvanized, HAZ, and fusion zone/weld metal (WM)

The average hardness values for the base metal for stainless and galvanized steel were 62.95 HRB and 64.65 HRB, respectively. There was a significant increase in hardness of stainless steel HAZ on average but it was not significant for the galvanized steel. An interesting observation was, however, made for the weld metal zone where a high hardness value was recorded in W1 with 76.50 HRB while a low value was found in W6 with 66.5 HRB. This was associated with the ability of higher current to produce higher heat. It was also discovered from the heat input equation [26] that the diameter of the electrode does not affect the amount of heat input. Meanwhile, it was electrically discovered that the diameter of the conducting wire normally affects the number of electrons passing through. This means a wire with a larger diameter is expected to have lower current resistance, thereby, leading to higher heat input during the welding. A similar finding has also been reported by Chandra et al. [36] that a wide electrode diameter produced higher heat on metal in Tungsten Inert Gas Welding. It can be stated that a high heat input usually leads to faster and higher production of heat which further causes the solidification and cooling rate to be longer or slower. Moreover, heat input and solidification rate affect grain roughness such that a higher heat input and slower solidification rate

is expected to make the grain size and grain size number to be coarser as indicated in **Figure 9**. This can further lead to a decrease in hardness. According to Hamd et al. [34], the microhardness of welded AISI 1015 plate increased as the weld heat input decreased. This means the hardness profile tends to increase at lower heat input [35]. This case shows that the heat is more diffuse or concentrated towards the galvanized steel than the stainless steel because its thermal conductivity is higher as presented in **Table 2**. Moreover, the average hardness of the HAZ in stainless steel in each variable was observed to be higher than the galvanized steel. It was also discovered that even though the grain size of stainless steel in base metal and HAZ was larger than galvanized steel as indicated in **Figure 9** the stainless steel had higher hardness. This is due to differences in the chemical composition of the alloy and the fact that hardness is influenced by grain size but more dominantly by the composition of the alloying elements as presented in **Table 1**, **Figure 8a**, and **Figure 8b**.

3.4. Tensile strength

The average tensile test results for each variable are presented in **Figure 11** and it was discovered that almost all the specimens broke in the weld and HAZ areas. Moreover, all the joint tensile strengths were observed to be lower than the base metal tensile strength. This proves that welded joints with dissimilar materials reduced the construction strength compared to one metal without welded joints.
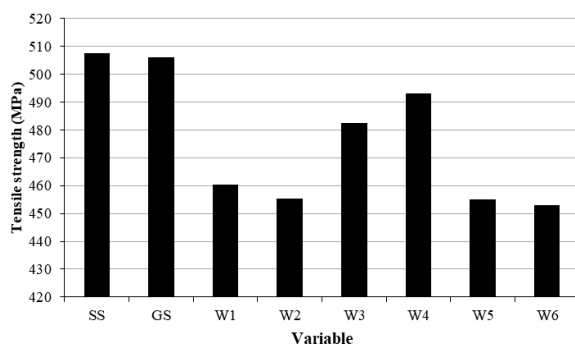

Figure 11. Average values of tensile strength for each testing variable

The tensile strength of the joint was found to be lower than the base metal as indicated by the 507.620 MPa recorded for stainless steel and 505.984 MPa for galvanized steel. This is due to the penetration of zinc in the weld pool. It is important to note that a faster cooling rate causes more zinc penetration to the weld pool, thereby, leading to lower tensile strength [37], [38]. In fusion welding, the base and filler metal are converted to a liquid state, and the melting point of iron is 1535 °C while the zinc layer liquifies at 419.5 °C and turns into a gas state at 907 °C [39]. This means the zinc vapor usually generated when welding galvanized steel sheet often causes unwanted porosity in the weld seam as indicated in **Figure 8c**, **Figure 8d,** and **Figure 8e**). The porosity further causes inhomogeneous deformation which normally accelerates failure and significantly lower ductility [40]. It is also important to note that the vaporized zinc layer was held up and diffused through the melting weld [41]–[43].

The lowest average tensile strength of 452.929 MPa was observed in W6 with 1.0 mm filler wire diameter, 110A current, and 534.285 J/mm heat input while the highest, 493,021 MPa, was W4 with 1.0 mm filler wire diameter, 90A current, and 437.143J/mm heat input. This trend contrasts with previous reports that lower weld current produced lower heat input and this subsequently increased hardness and tensile strength during the dissimilar welding of ultrahigh strength steel and duplex stainless steel [35].

4. Conclusion

The welding of two different metals also known as dissimilar materials during bus body construction requires special treatment. This research analyzed the macrostructure, hardness, and tensile strength of dissimilar material welding joints through stainless and galvanized steels joined using GMAW. The current was varied at 90, 100, and 110 A while different diameters of ER70S-6 filler wire were used at 0.8 and 1.0 mm. The results showed that:

a. A welding wire with a larger diameter and higher current produced greater heat input which led to wider capping and deeper weld penetration.

b. Acicular and Widmanstatten ferrite phases were formed in the heat-affected zones of both the stainless and galvanized steels. It was discovered that larger filler wire diameter and higher current produced more Widmanstatten ferrite phase. Meanwhile, the martensite-bainite phase was visible on the weld metal.

The findings also showed that grain boundary roughening occurred along the HAZ and WM as the diameter of the welding wire and the current increased.

c. The hardness of HAZ and WM was affected by the grain size and grain size number. Moreover, larger filler wire diameter and higher current produced higher heat input on the metal. This subsequently slowed down the solidification and cooling rate, thereby, making the grain size coarser.

d. The average tensile strength of welded joints was found to be lower than the value for the base metal. This is due to the changes in the HAZ structure. Therefore, further studies are needed to increase the strength of the dissimilar material welding joints to be the same as the base metal.

Finally, the results of this research provide evidence and new insights in the field of welding technology, especially to be applied to the bus body industry.

Acknowledgment

_____

Author's Declaration

Authors' contributions and responsibilities

The authors made substantial contributions to the conception and design of the study. The authors took responsibility for data analysis, interpretation, and discussion of results. The authors read and approved the final manuscript.

Funding

No funding information from the authors.

Availability of data and materials

All data are available from the authors.

Competing interests

The authors declare no competing interest.

Additional information

No additional information from the authors.

_____

References

[1] D. W. Karmiadji, M. Gozali, M. Setiyo, T. Raja, and T. A. Purnomo, "Comprehensive Analysis of Minibuses Gravity Center: A Post-Production Review for Car Body Industry," *Mechanical Engineering for Society and Industry*, vol. 1, no. 1, pp. 31–40, 2021, doi: 10.31603/mesi.5250.

[2] G. Refiadi, I. S. Aisyah, and J. P. Siregar, "Trends in lightweight automotive materials for improving fuel efficiency and reducing carbon emissions," *Automotive Experiences*, vol. 2, no. 3, pp. 78–90, 2019, doi: 10.31603/ae.v2i3.2984.

[3] U. Dilthey and L. Stein, "Multimaterial car body design: challenge for welding and joining," *Science and Technology of Welding and Joining*, vol. 11, no. 2, pp. 135–142, Mar. 2006, doi: 10.1179/174329306X85967.

[4] N. T. Switzner and Z. Yu, "Austenitic Stainless Steel Cladding Interface Microstructures Evaluated for Petrochemical Applications," *Welding Journal*, vol. 98, p. 50s, Feb. 2019, doi: 10.29391/2019.98.004.

[5] J. Wang, M. Lu, L. Zhang, W. Chang, L. Xu, and L. Hu, "Effect of welding process on the microstructure and properties of dissimilar weld joints between low alloy steel and duplex stainless steel," *International Journal of Minerals, Metallurgy, and Materials*, vol. 19, no. 6, pp. 518–524, 2012, doi: 10.1007/s12613-012-0589-z.

[6] A. M., C. Das Vemulapalli, and M. Cheepu, "Effect of filler materials on dissimilar TIG welding of Inconel 718 to high strength steel," *Materials Today: Proceedings*, vol. 52, pp. 1314–1320, 2022, doi: https://doi.org/10.1016/j.matpr.2021.11.061.

[7] C. H. Kuo, K. H. Tseng, and C. P. Chou, "Effect of Activated TIG Flux on Performance of Dissimilar Welds between Mild Steel and Stainless Steel," *Key Engineering Materials*, vol. 479, pp. 74–80, 2011, doi: 10.4028/www.scientific.net/KEM.479.74.

[8] M. Sireesha, V. Shankar, S. K. Albert, and S. Sundaresan, "Microstructural features of dissimilar welds between 316LN austenitic stainless steel and alloy 800," *Materials Science and Engineering: A*, vol. 292, no. 1, pp. 74–82, 2000, doi: https://doi.org/10.1016/S0921-5093(00)00969-2.

[9] S. Chowdhury *et al.*, "Comparison of microstructure and mechanical performance

of laser and electron beam welded Ti6Al4V alloy," *Journal of the Brazilian Society of Mechanical Sciences and Engineering*, vol. 43, no. 3, p. 173, 2021, doi: 10.1007/s40430-021-02903-y.

[10] P. Boobalakrishnan *et al.*, "Thermal management of metal roof building using phase change material (PCM)," *Materials Today: Proceedings*, vol. 47, pp. 5052–5058, 2021, doi: https://doi.org/10.1016/j.matpr.2021.05.012.

[11] K. B. Prakash, C. Subramaniayan, M. Chandrasekaran, P. Manoj Kumar, and S. Saravanakumar, "Development of mathematical model to study the effect of indoor air quality parameters and optimization using response surface methodology," *Materials Today: Proceedings*, vol. 45, pp. 8195–8198, 2021, doi: https://doi.org/10.1016/j.matpr.2021.03.087.

[12] V. García-García, "Microstructural and mechanical analysis of double pass dissimilar welds of twinning induced plasticity steel to austenitic/duplex stainless steels," *International Journal of Pressure Vessels and Piping*, vol. 198, p. 104665, 2022, doi: https://doi.org/10.1016/j.ijpvp.2022.104665.

[13] A. K. Maurya, C. Pandey, and R. Chhibber, "Dissimilar welding of duplex stainless steel with Ni alloys: A review," *International Journal of Pressure Vessels and Piping*, vol. 192, p. 104439, 2021, doi: https://doi.org/10.1016/j.ijpvp.2021.104439.

[14] S. Tathgir, D. W. Rathod, and A. Batish, "Emphasis of Weld Time, Shielding Gas and Oxygen Content in Activated Fluxes on the Weldment Microstructure," *Mechanical Engineering for Society and Industry*, vol. 1, no. 2, pp. 86–95, 2021.

[15] M. Jafarzadegan, A. H. Feng, A. Abdollah-zadeh, T. Saeid, J. Shen, and H. Assadi, "Microstructural characterization in dissimilar friction stir welding between 304 stainless steel and st37 steel," *Materials Characterization*, vol. 74, pp. 28–41, 2012, doi: https://doi.org/10.1016/j.matchar.2012.09.004.

[16] Z. Zhang, X. Wang, Q. Sun, B. Yang, L. Xiong, and H. Liu, "Study on microstructure and properties of laser dissimilar welded joints of ultra-high strength PHS1500/PHS2000 steel,"

Optics & Laser Technology, vol. 150, p. 107933, 2022, doi: https://doi.org/10.1016/j.optlastec.2022.10793 3.

[17] J. Xin *et al.*, "The microstructures and mechanical properties of dissimilar laser welding of copper and 316L stainless steel with Ni interlayer," *Cryogenics*, vol. 118, p. 103344, 2021, doi: https://doi.org/10.1016/j.cryogenics.2021.103 344.

[18] T. E. Abioye, O. E. Ariwoola, T. I. Ogedengbe, P. K. Farayibi, and O. O. Gbadeyan, "Effects of Welding Speed on the Microstructure and Corrosion Behavior of Dissimilar Gas Metal Arc Weld Joints of AISI 304 Stainless Steel and Low Carbon Steel," *Materials Today: Proceedings*, vol. 17, pp. 871–877, 2019, doi: https://doi.org/10.1016/j.matpr.2019.06.383.

[19] M. Vahman, M. Shamanian, M. A. Golozar, A. Jalali, M. A. Sarmadi, and J. Kangazian, "The Effect of Welding Heat Input on the Structure–Property Relationship of a New Grade Super Duplex Stainless Steel," *steel research international*, vol. 91, no. 1, p. 1900347, Jan. 2020, doi: https://doi.org/10.1002/srin.201900347.

[20] M. Ramarao, M. F. L. King, A. Sivakumar, V. Manikandan, M. Vijayakumar, and R. Subbiah, "Optimizing GMAW parameters to achieve high impact strength of the dissimilar weld joints using Taguchi approach," *Materials Today: Proceedings*, vol. 50, pp. 861–866, 2022, doi: https://doi.org/10.1016/j.matpr.2021.06.137.

[21] U. S. Patil and M. S. Kadam, "Microstructural analysis of SMAW process for joining stainless steel 304 with mild steel 1018 and parametric optimization by using response surface methodology," *Materials Today: Proceedings*, vol. 44, pp. 1811–1815, 2021, doi: 10.1016/j.matpr.2020.12.008.

[22] A. Gullino, P. Matteis, and F. D'Aiuto, "Review of aluminum-to-steel welding technologies for car-body applications," *Metals*, vol. 9, no. 3, p. 315, 2019.

[23] ISO 5817, "International Standard ISO (Welding — Fusion-welded joints in steel, nickel, titanium and their alloys)," vol. 2014, 2014.

[24] C. Steel, *Cobelco Welding Handbook*. Cobelco welding of America Inc, USA, 1991.

[25] W. D. Callister and J. Wiley, *Materials Science*.

[26] S. Kou, *Welding Metallurgy*, Second Edi. Hoboken, New Jersey: John Wiley & Sons, Inc., 2003.

[27] ASTM E112, "Standard Test Methods for Determining Average Grain Size 1," *Annual Book of ASTM Standard*, pp. 1–27, 2021, doi: 10.1520/E0112-12.1.4.

[28] ASTM E8, "Standard test methods for tension testing of metallic materials," *Annual Book of ASTM Standards 4*, no. C, pp. 1–27, 2010, doi: 10.1520/E0008.

[29] R. Demarque, E. P. Santos, R. S. Silva, and J. A. De Castro, "Evaluation of the effect of the thermal cycle on the characteristics of welded joints through the variation of the heat input of the austhenitic AISI 316L steels by the GMAW process," *Science and Technology of Materials*, vol. 30, pp. 51–59, 2018, doi: 10.1016/j.stmat.2018.09.001.

[30] N. Ghosh, P. K. Pal, and G. Nandi, "Parametric Optimization of MIG Welding on 316L Austenitic Stainless Steel by Grey-based Taguchi Method," *Procedia Technology*, vol. 25, pp. 1038–1048, 2016, doi: https://doi.org/10.1016/j.protcy.2016.08.204.

[31] H. Pouraliakbar, M. Hamedi, A. Hossein, and A. Nazari, "Designing of CK45 Carbon Steel and AISI 304 Stainless Steel Dissimilar Welds," vol. 17, no. 1, pp. 106–114, 2014.

[32] N. Switzner, H. Queiroz, J. Duerst, and Z. Yu, "Si-bronze to 304 stainless steel GTA weld fusion zone microstructure and mechanical properties," *Materials Science and Engineering: A*, vol. 709, pp. 55–64, 2018, doi: https://doi.org/10.1016/j.msea.2017.09.025.

[33] K. Easterling, *Introduction to the Physical Metallurgy of Welding*, 2 nd. Oxford: Butterworth Heinmann Ltd., 1992.

[34] E. K. Hamd, A. S. Alwan, and I. K. Irthiea, "Study the Effect of Welding Heat Input on the Microstructure, Hardness, and Impact Toughness of AISI 1015 Steel," *Al-Khwarizmi Engineering Journal*, vol. 14, no. 1, pp. 118–127, 2018, doi: 10.22153/https://doi.org/10.22153/kej.2018.08.005.

[35] H. Tasalloti Kashani, M. Dabiri, P. Kah, and J. Martikainen, "Effect of GMAW Heat Input on the Microstructure and Mechanical and Fatigue Behavior of Dissimilar Welds of Ultrahigh Strength Steel and Duplex Stainless Steel," 2017, doi: 10.1115/OMAE2017-62646.

[36] B. R. Chandra, S. Arul, and R. Sellamuthu, "Effect of Electrode Diameter and Input Current on Gas Tungsten Arc Welding Heat Distribution Parameters," *Procedia Materials Science*, vol. 5, pp. 2369–2375, 2014, doi: https://doi.org/10.1016/j.mspro.2014.07.481.

[37] P. Shreyas, B. Panda, and R. Kumar, "Mechanical properties and microstructure of 316L-galvanized steel weld," *Materials Today: Proceedings*, vol. 23, pp. 600–607, 2020, doi: https://doi.org/10.1016/j.matpr.2019.05.418.

[38] I. C. Okafor, R. J. O. Malley, K. R. Prayakarao, and H. A. Aglan, "Effect of Zinc Galvanization on the Microstructure and Fracture Behavior of Low and Medium Carbon Structural Steels," *Engineering*, vol. 5, no. 8, pp. 656–666, 2013.

[39] M. Sarpe, K. Treutler, V. Wesling, P. Dewald, and H. C. Schmale, "Influence of classified pore contents on the quasi-static and cyclic strength properties of the welded joint in gas-shielded metal arc welding of galvanized, high-strength steels," *Journal of Advanced Joining Processes*, vol. 5, no. December 2021, p. 100094, 2022, doi: 10.1016/j.jajp.2021.100094.

[40] E. He *et al.*, "Effect of porosities on tensile properties of laser-welded Al-Li alloy: an experimental and modelling study," *The International Journal of Advanced Manufacturing Technology*, vol. 95, no. 1, pp. 659–671, 2018, doi: 10.1007/s00170-017-1175-3.

[41] M. Takenouchi and T. Shimizu, "Arc welding of surface treated steel plates," *Welding International*, vol. 6, no. 5, pp. 351–355, Jan. 1992, doi: 10.1080/09507119209548201.

[42] S. Izutani, K. Yamazaki, and R. Suzuki, "New welding process, 'j-Solution™ Zn,' suitable for galvanized steel in the automotive industry," *R and D: Research and Development Kobe Steel Engineering Reports*, vol. 63, no. 1, pp. 54–59, 2013.

[43] H. Matsui, H. Suzuki, and M. Yamada, "Reduction of blowholes in high-speed arc welding of hot-dip galvanised steel sheets," *Welding International*, vol. 12, no. 6, pp. 432–439, Jan. 1998, doi: 10.1080/09507119809448511.